Geophysical Research Letters

RESEARCH LETTER
10.1029/2020GL087948

Insolation and Greenhouse Gas Forcing of the South American Monsoon System Across Three Glacial-Interglacial Cycles

Alicia Hou[1], André Bahr[1], Jacek Raddatz[2], Silke Voigt[2], Markus Greule[1], Ana Luiza Albuquerque[3], Cristiano M. Chiessi[4], and Oliver Friedrich[1]

[1]Institute of Earth Sciences, Heidelberg University, Heidelberg, Germany, [2]Institute of Geosciences, Goethe University Frankfurt, Frankfurt, Germany, [3]Programa de Geociências (Geoquímica), Universidade Federal Fluminense, Niterói, Brazil, [4]School of Arts, Sciences and Humanities, University of São Paulo, São Paulo, Brazil

Abstract Precipitation extremes with devastating socioeconomic consequences within the South American Monsoon System (SAMS) are expected to become more frequent in the near future. The complexity in SAMS behavior, however, poses severe challenges for reliable future projections. Thus, robust paleomonsoon records are needed to constrain the high spatiotemporal variability in the response of SAMS rainfall to different climatic drivers. This study uses Ti/Ca ratios from X-ray fluorescence scanning of a sediment core retrieved off eastern Brazilian to trace precipitation changes over the past 322 Kyr. The results indicate that despite the spatiotemporal complexity of the SAMS, insolation forcing is the primary pacemaker of variations in the monsoonal system. Additional modulation by atmospheric pCO_2 suggests that SAMS intensity over eastern Brazil will be suppressed by rising CO_2 emissions in the future. Lastly, our record reveals an unprecedented strong and persistent wet period during Marine Isotope Stage 6 driven by anomalously strong trade winds.

Key Points:
- Insolation is the main driver of orbital-scale South American Monsoon System rainfall variability in eastern Brazil over the past 322 kyr
- Monsoonal rainfall intensity is indirectly modulated by greenhouse gas forcing through changes to the latitudinal temperature gradients
- During MIS 6, precipitation in eastern Brazil remained anomalously strong and deviated from the regular orbitally paced insolation forcing

Supporting Information:
- Supporting Information S1

Correspondence to:
A. Hou,
alicia.hou@geow.uni-heidelberg.de

Citation:
Hou, A., Bahr, A., Raddatz, J., Voigt, S., Greule, M., Albuquerque, A. L., et al. (2020). Insolation and greenhouse gas forcing of the South American Monsoon System across three glacial-interglacial cycles. *Geophysical Research Letters*, *46*, e2020GL087948. https://doi.org/10.1029/2020GL087948

Received 12 MAR 2020
Accepted 6 JUL 2020
Accepted article online 8 JUL 2020

1. Introduction

Over a broad region of South America, low-level atmospheric circulation and convective precipitation during austral summer are governed by the South American Monsoon System (SAMS) (Liebmann & Mechoso, 2011; Zhou & Lau, 1998). SAMS precipitation affects the basins of several major rivers in Brazil (e.g., Amazon, São Francisco, and Paraná), some of which are densely populated and intensively exploited. As such, monsoon-related hydrological extremes may have disastrous consequences for human livelihood, agriculture, energy production, and infrastructure (Marengo et al., 2012). A recent review by Pascale et al. (2019) suggests that while the core of the SAMS will likely migrate southward under continuing greenhouse gas (GHG) emissions, there is still uncertainty regarding projected precipitation changes for much of the SAMS domain. Therefore, it is an urgent task to better understand how SAMS rainfall responds to different climatic drivers, including GHG forcing.

The onset of peak SAMS activity occurs during austral summer when strong heating over central South America enhances the prevailing northeast (NE) trade winds which transport moist air from the tropical North Atlantic Ocean toward the continent (Silva & Kousky, 2012; Zhou & Lau, 1998). This moist air mass is deflected by the Andes and then heads southeastward toward the South Atlantic Convergence Zone (SACZ) (Gan et al., 2004; Zhou & Lau, 1998), a convective belt that extends from the western Amazon basin toward southeastern (SE) South America and into the western South Atlantic Ocean (Carvalho et al., 2002, 2004) (Figure 1). Monsoon development begins in austral spring, reaches its mature phase during austral summer, and recedes in austral fall (Marengo et al., 2001; Vera et al., 2006). Across much of tropical South America, over 40% of the total annual precipitation occurs during the mature SAMS phase (Figure 1).

Available long-term records of SAMS precipitation reveal the dominant influence of precession-paced austral summer insolation changes on monsoonal rainfall intensity (Cheng et al., 2013; Cruz et al., 2005; Govin et al., 2014). However, distinct out-of-phase precipitation changes between western Amazonia and SE Brazil versus eastern Amazonia and NE Brazil over the past 250 Kyr indicate high spatial variability in rainfall intensity within the core SAMS domain (Cheng et al., 2013; Govin et al., 2014).

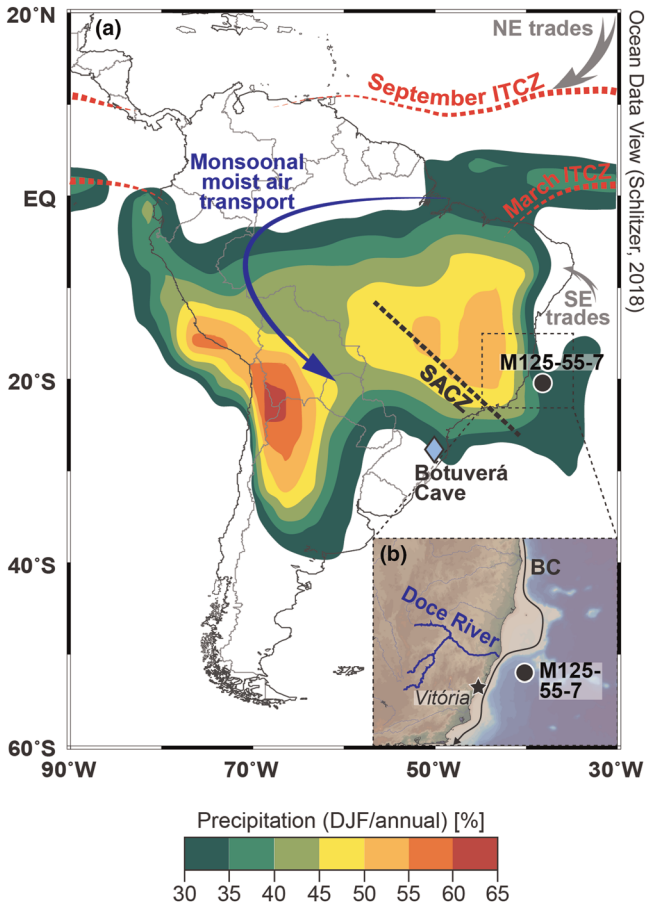

Figure 1. (a) Percentage of annual precipitation during the active South American Monsoon System (SAMS) phase (December-January-February [DJF]) based on Climate Prediction Center Merged Analysis of Precipitation data (1979–2004) (Xie & Arkin, 1997; figure adapted from Vuille et al., 2012). Locations of Site M125-55-7 (this study; black circle) and Botuverá Cave (blue diamond; Cruz et al., 2005) are indicated. Also shown are the modern mean seasonal positions of the Intertropical Convergence Zone (ITCZ; red dashed lines), mean climatological position of the South Atlantic Convergence Zone (SACZ; black dashed line), and the path of moist air during the active SAMS phase (blue arrow). The sizes of the gray arrows correspond to the relative strengths of the northeast and southeast trade winds during the mature SAMS phase. (b) The main tributaries of the Doce River, locations of Site M125-55-7 (this study; black circle) and the nearby city of Vitória (red star), and the flow path of the Brazil Current (BC; after Aguiar et al., 2014).

This study aims to disentangle the complexity in the SAMS by investigating the climatic drivers of long-term monsoonal rainfall variability at the NE extent of the SACZ, where rainfall intensity is likely sensitive to spatial shifts in the monsoon system. We present the longest record of the SAMS yet published by using Ti/Ca ratios from a marine sediment core retrieved off the coast of tropical eastern Brazil, coupled with planktic foraminiferal stable isotopes to reconstruct changes in monsoonal precipitation intensity across three glacial-interglacial cycles. The new record allows us to assess the potential roles of austral summer insolation, atmospheric pCO_2, and latitudinal SST gradients in modulating SAMS rainfall intensity.

2. Regional Setting

Site M125-55-7 lies within the southward flowing Brazil Current, near the mouth of the Doce River, which is the dominant source of terrigenous sediments to the core location (Figure 1). Climate in the Doce basin is humid (sub)tropical with temperate or hot summers and dry winters, except in the coastal lowlands where a tropical monsoon climate prevails (Alvares et al., 2013). Sediment outflow from the Doce River is dependent on rainfall amount and is highest during the austral summer rainy season (Oliveira & da Silva Quaresma, 2017). Along the coast, precipitation proceeds throughout austral winter due to the landward advection of moist air by the prevailing SE trade winds (Vera et al., 2002).

3. Methods

3.1. Core M125-55-7

Piston Core M125-55-7 was raised from 1,960.8 m depth off the coast of eastern Brazil (20°21.807′S, 38°37.387′W) in March/April 2016 during RV METEOR cruise M125 (Bahr et al., 2016) (Figure 1). The 1,175 cm long piston core contains bioclast-bearing clay to silty clay, alternates between dark and light gray in color, and lacks visible hiatuses (Bahr et al., 2016). We use the age model from Hou et al. (2020), which is based on ^{14}C dating and tuning of the benthic $\delta^{18}O$ record to the LR04 benthic $\delta^{18}O$ stack (associated with a 4 Kyr age uncertainty) (Lisiecki & Raymo, 2005). Core M125-55-7 spans the past 322 Kyr and has a mean sedimentation rate of 4 cm/Kyr.

3.2. XRF Scanning

The archive halves of the split cores were scanned using the fourth generation AVAATECH X-ray fluorescence (XRF) core scanner at the Institute of Earth Sciences, Heidelberg University. Elemental intensities were measured every 5 mm for 20 s at 10 kV using a slit size of 5 mm downcore and 12 mm crosscore. The surface of the sediment was smoothed and covered with a 4 μm thick Ultralene® foil to avoid contamination of the detector window and desiccation of the sediment. Processing of the raw XRF data was performed using the bAxilBatch software (Version 1.4, July 2016; www.brightspec.be). The mean temporal resolution of the XRF data is ~125 years.

3.3. Stable Isotope Analysis

Ten cubic centimeters of sediment was sampled at ~2.5 cm resolution. The samples were freeze dried, wet sieved over a 63 μm mesh, and oven dried overnight. Thirty to 40 *Globigerinoides ruber* (pink) specimens were selected from each sample and gently crushed to open shell chambers. The aliquot of cracked *G. ruber* (pink) tests designated for stable isotope analysis was rinsed three times with ultrapure methanol

and briefly ultrasonicated between rinses. Stable isotopes were measured with a Thermo Fisher Scientific MAT 253plus mass spectrometer coupled to a Kiel IV carbonate preparation line at the Institute of Earth Sciences, Heidelberg University (Germany). An in-house carbonate standard (Solnhofen limestone) calibrated against the reference material IAEA-603 (calcite; $\delta^{18}O_{VPDB} = -2.37 \pm 0.04‰$) was used to normalize measured raw $\delta^{18}O$ values to the VPDB isotope reference scale. The analytical precision for $\delta^{18}O$ is better than 0.054‰ (1σ) based on replicate measurements ($n = 23$) of the in-house standard.

3.4. Ice-Volume-Free Seawater Oxygen Isotopic Composition ($\delta^{18}O_{IVF\text{-}SW}$) Calculation

Seawater $\delta^{18}O$ composition ($\delta^{18}O_{SW}$) was estimated with the temperature-$\delta^{18}O$ relationship of Mulitza et al. (2003) [SST = 14.2 − 4.44 ($\delta^{18}O_C - \delta^{18}O_{SW}$)], using *G. ruber* (pink) $SST_{Mg/Ca}$ (Hou et al., 2020) and $\delta^{18}O_{G.\ ruber}$. $\delta^{18}O_{IVF\text{-}SW}$, a proxy for sea surface salinity, was computed by removing the effect of global ice volume on $\delta^{18}O_{SW}$ using the ice volume reconstruction of de Boer et al. (2014). The estimated cumulative error for $\delta^{18}O_{IVF\text{-}SW}$ values is ±0.27‰ and includes the 1.2°C uncertainty of the Mg/Ca-SST equation (Dekens et al., 2002), the analytical precision for $\delta^{18}O$, and the 0.116‰ uncertainty of the ice-volume correction (de Boer et al., 2014).

3.5. River and Seawater $\delta^{18}O$ Analyses

$\delta^{18}O$ analysis of seawater and river samples was performed at the GeoZentrum, Nordbayern, University of Erlangen-Nürnberg, Germany. Samples were analyzed by an automated equilibration unit (Thermo Fisher Scientific Gasbench 2) in continuous flow mode coupled to a Thermo Fisher Scientific Delta *plus* XP isotope ratio mass. All samples were measured in triplicates, and the reported value is the mean. Values are reported in the standard delta notation in per mil (‰) versus Vienna Standard Mean Ocean (VSMOW) following Coplen (2011). The data were corrected for instrumental drift and normalized to the VSMOW/Standard Light Antarctic Precipitation scale by assigning a value of 0‰ and −55.5‰ ($\delta^{18}O$) to VSMOW2 and Standard Light Antarctic Precipitation 2, respectively (Brand et al., 2014). External reproducibility based on repeated analyses of a control sample was better than 0.1‰ ($\pm 1\sigma$).

3.6. Spectral Analyses

Multitaper method spectral analysis (Thomson, 1982) and Evolutive Harmonic Analysis of the evenly interpolated (130 year resolution) and linearly detrended M125-55-7 ln (Ti/Ca) record were performed using the R package "astrochron" (Meyers, 2014). Using a taner window (minimum frequency = 0.056, maximum frequency = 0.04, and roll-off rate = 10^5), we performed band-pass filtering of precession frequencies from the ln (Ti/Ca) record and notch filtering of the precession frequencies from the ln (Ti/Ca) record to produce a precession-free ln (Ti/Ca) record. Using the R package "biwavelet" (Gouhier et al., 2019), we analyzed the wavelet transform coherence between the evenly interpolated (600 year resolution) M125-55-7 ln (Ti/Ca) and $\delta^{18}O_{IVF\text{-}SW}$ time series over 1,000 Monte Carlo randomizations.

4. Results and Discussion

4.1. Interpretation of ln (Ti/Ca) Ratios

Marine sediment cores from near-shore settings are ideally suited for reconstructing past variations in terrigenous sediment input related to precipitation changes in the hinterland (Govin et al., 2012, 2014). The Ti/Ca ratio of marine sediments can be used to trace the relative proportion of terrigenous siliciclastic components versus marine biogenic carbonate (Arz et al., 1998; Peterson et al., 2000; Rothwell & Croudace, 2015). Previous studies have successfully employed the Ti/Ca ratio as a proxy for fluvial terrigenous runoff, for example, to reconstruct continental precipitation changes offshore Northeastern Brazil (Arz et al., 1998; Jaeschke et al., 2007; Mulitza et al., 2017). Using Ti to represent terrigenous input by the Doce River is further corroborated by a principal component analysis of the elemental composition of the sediment performed using the program PAST 3.20 (Hammer et al., 2001; see supporting information Text S1 and Figures S1 and S2). Generally, low ln (Ti/Ca) values co-occur with warm Marine Isotope Stage (MIS) substages, while high ln (Ti/Ca) values coincide with cold MIS substages (Figure 2). The variability in ln (Ti/Ca) ratios prominently displays pacing that is in phase with orbital precession, albeit with notably damped amplitude during MIS 6 (see section 4.4).

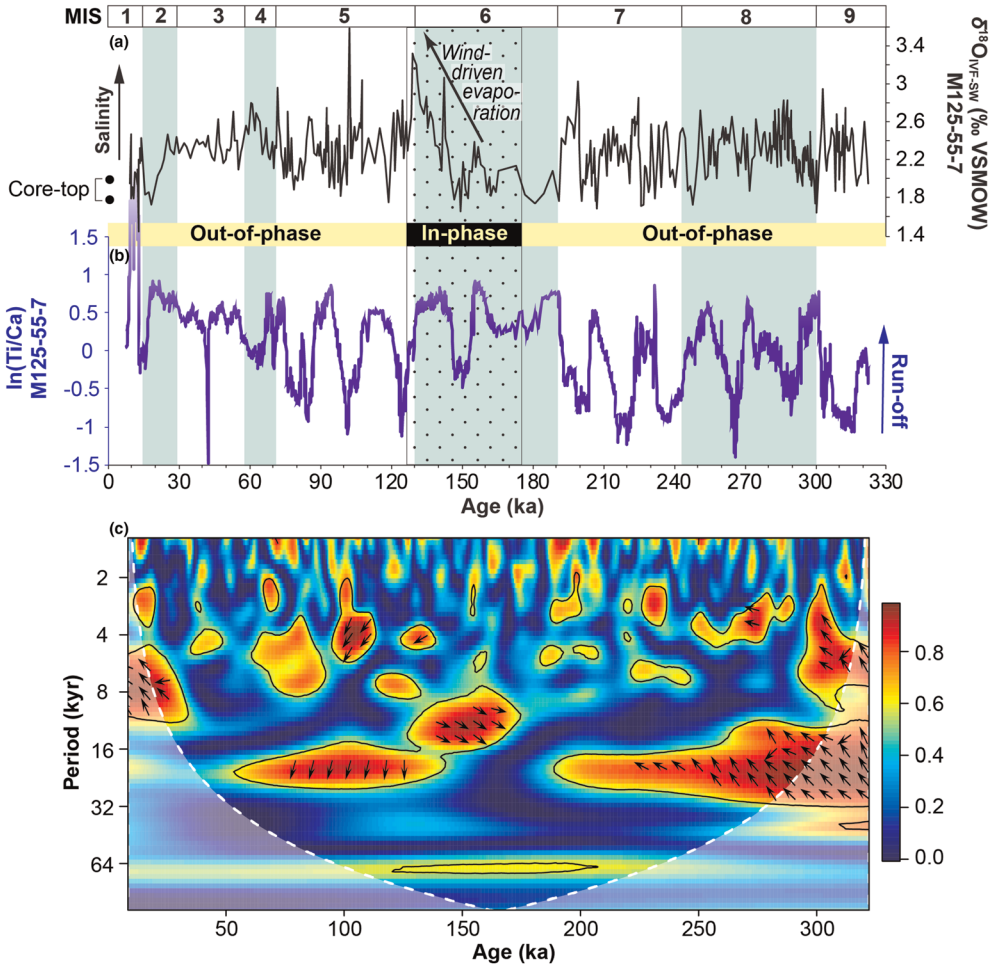

Figure 2. (a) Site M125-55-7 ice-volume-free seawater oxygen isotopic composition ($\delta^{18}O_{IVF\text{-}SW}$; black line) based on *Globigerinoides ruber* (pink) $\delta^{18}O$ and Mg/Ca (Hou et al., 2020) and (b) ln (Ti/Ca) ratios from X-ray fluorescence scanning (blue line). Green bars and numbers at the top denote Marine Isotope Stages (MIS). (c) Wavelet coherence between Site M125-55-7 $\delta^{18}O_{IVF\text{-}SW}$ values and ln (Ti/Ca) ratios, zero phase lag is represented by arrows pointing to the right.

Given the near-coast locality of Site M125-55-7, terrestrial input variability may be sensitive to changes in sea level (Govin et al., 2014; Rühlemann et al., 1996). We expect ln (Ti/Ca) values to be lower during sea level high stands, when there is less erodible shelf area and the sediment source is distant from the continental slope due to retrograding sedimentary systems (and vice versa for sea level lowstands). However, the seismic stacking pattern at Site M125-55-7 and the comparison of our ln (Ti/Ca) record with benthic $\delta^{18}O$ values from the same core (Hou et al., 2020) do not indicate a strong influence of sea level fluctuations on ln (Ti/Ca) values (see Text S2 and Figures S3 and S4). ln (Ti/Ca) ratios may also be affected by changes in marine productivity, which alters the relative proportion of biogenic carbonates in marine sediments (Govin et al., 2012, 2014). However, given the dominance of oligotrophic Tropical Water in the photic zone near Site M125-55-7 (de Castro et al., 2006) and the lack of correlation between ln (Ti/Ca) values and the productivity-dependent *G. ruber* (pink) $\delta^{13}C$ record from the same core (Figure S3), we propose that the variability in ln (Ti/Ca) ratios is not strongly affected by changes in the biogenic carbonate component. Carbonate dissolution is also unlikely to influence our ln (Ti/Ca) ratios since Site M125-55-7 (1,960.8 m) is located well above the modern (~4,000 m) and glacial (~3,500 m) lysocline in the western South Atlantic (Volbers & Henrich, 2004).

To further evaluate the robustness of our ln (Ti/Ca) record as a terrigenous runoff proxy, we compared it with the $\delta^{18}O_{IVF\text{-}SW}$ record based on *G. ruber* (pink) specimens from the same core (Figure 2). The records

reveal a statistically robust correlation (Figure S5a) indicating that when sediment input from the Doce River is high, offshore sea surface $\delta^{18}O_{IVF\text{-}SW}$ (a proxy for surface salinity [SSS]) is low. Today, the influence of Doce River fluvial discharge on the $\delta^{18}O_{water}$ composition of oceanic surface water is confined to the near-shore region (see Text S3, Figure S6, and Table S1) and therefore plays a minimal role in SSS changes near Site M125-55-7. Instead, we infer that the reconstructed variability in SSS at our site is more dependent on changes in the rate of surface evaporation (Bahr et al., 2013), which, among other factors, is strongly influenced by cloudiness. Therefore, an increase in convective cloudiness over eastern Brazil and the nearby oceanic region may reduce offshore evaporation rates and SSS while simultaneously intensifying continental precipitation and runoff. Oceanic evaporation and SSS are also influenced by changes in surface wind stress (Yu, 2007), where an increase in wind stress leads to an increase in the rate of evaporation and higher SSS. Notably, we observe a diversion from the otherwise out-of-phase relationship in the precession band (~21 Kyr) between ln (Ti/Ca) and $\delta^{18}O_{ivf\text{-}sw}$ during ~125–175 ka (based on the wavelet transform coherence; Figure 2b), when the two records are almost perfectly in-phase. This anomalous relationship during MIS 6 may be a consequence of exceptionally strong SE trade winds during MIS 6 (Hou et al., 2020) (see ; section 4.4).

4.2. Insolation Forcing

In agreement with previous proxy- and modeling-based monsoonal studies (e.g., Cheng et al., 2012; Kutzbach, 1981), we observe a tight coupling between ln (Ti/Ca) values and precession-paced austral summer insolation cycles (Laskar et al., 2004) and find dominant peaks in power at 23 Kyr based on spectral analysis of the ln (Ti/Ca) record (Figures 3a, 3b, and S7). Our results also reveal that the sensitivity of precipitation over the Doce Basin to insolation forcing is higher when the amplitude of precession is large (e.g., MIS 5) and lower when precession is weak (e.g., MIS 2–4). Thus, we infer that both the amplitude and frequency of fluctuations in the ln (Ti/Ca) record are modulated by precession-paced insolation changes over the past 322 Kyr. During maxima in austral summer insolation, differences in land-sea heat capacity produce stronger thermal gradients, which lead to intense convection and precipitation over the continent (Silva & Kousky, 2012). During MIS 6e–c, however, the amplitude of the ln (Ti/Ca) fluctuations are muted compared to those of the insolation cycles, indicating that continental precipitation and runoff changes occurring in eastern Brazil during this period are likely modulated by other drivers (see section 4.4).

Comparison of our Southern Hemisphere ln (Ti/Ca) record to the Northern Hemisphere East Asian Summer Monsoon (Cheng et al., 2009; Dykoski et al., 2005; Kelly et al., 2006; Wang et al., 2001, 2008; Yuan et al., 2004) reveals a long-term precession-paced antiphasing, consistent with insolation as the primary modulator of the intensity of (sub)tropical monsoons (Cheng et al., 2012; Kutzbach et al., 2008) (Figure 3). However, the periodic mismatch (e.g., during MIS 3) between our ln (Ti/Ca) record and the speleothem $\delta^{18}O$ record from Botuverá Cave (subtropical SE Brazil) (Cruz et al., 2005) reveals precipitation differences within the SAMS domain, despite the shared insolation influence (Figure 3b). Thus, while our data suggest that insolation has been the primary driver of SAMS variability on orbital time scales for the past 322 Kyr, deviations in the shape and amplitude of our ln (Ti/Ca) record from orbital precession elude to modulation by other, superimposed drivers of precipitation variability in eastern Brazil. As discussed in the following, we infer that these overprinting factors might be directly and indirectly coupled to GHG forcing.

4.3. GHG Forcing

To investigate the influence of past changes in GHG concentration on monsoonal rainfall over the Doce Basin, we compared our precession-free ln (Ti/Ca) record (Figure 4d) to atmospheric pCO_2 changes (EPICA Dome C: Monnin et al., 2001; Voskok: Petit et al., 1999) (Figure 4a). Although we find that an increase in GHG concentrations is associated with a statistically significant decrease in precipitation, the large differences in amplitude between the ln (Ti/Ca) and atmospheric pCO_2 records point to nonlinear feedbacks (Figure S5b). Since modeling studies stipulate that a doubling of CO_2 concentration lowers latitudinal temperature gradients (Rind, 1998, 2000), we assess the ability of GHG forcing to indirectly modulate SAMS intensity through changes to the interhemispheric and intrahemispheric latitudinal temperature gradients. To test this hypothesis, we computed the correlations between the precession-free ln (Ti/Ca) record from M125-55-7, GHG concentrations, and the interhemispheric and intrahemispheric SST gradients (Figures 4 and S5c–S5f). The interhemispheric temperature gradient is based on the difference between the IODP Site U1313 (midlatitude North Atlantic) alkenone-based SST record (Naafs et al., 2012) and the Site M125-

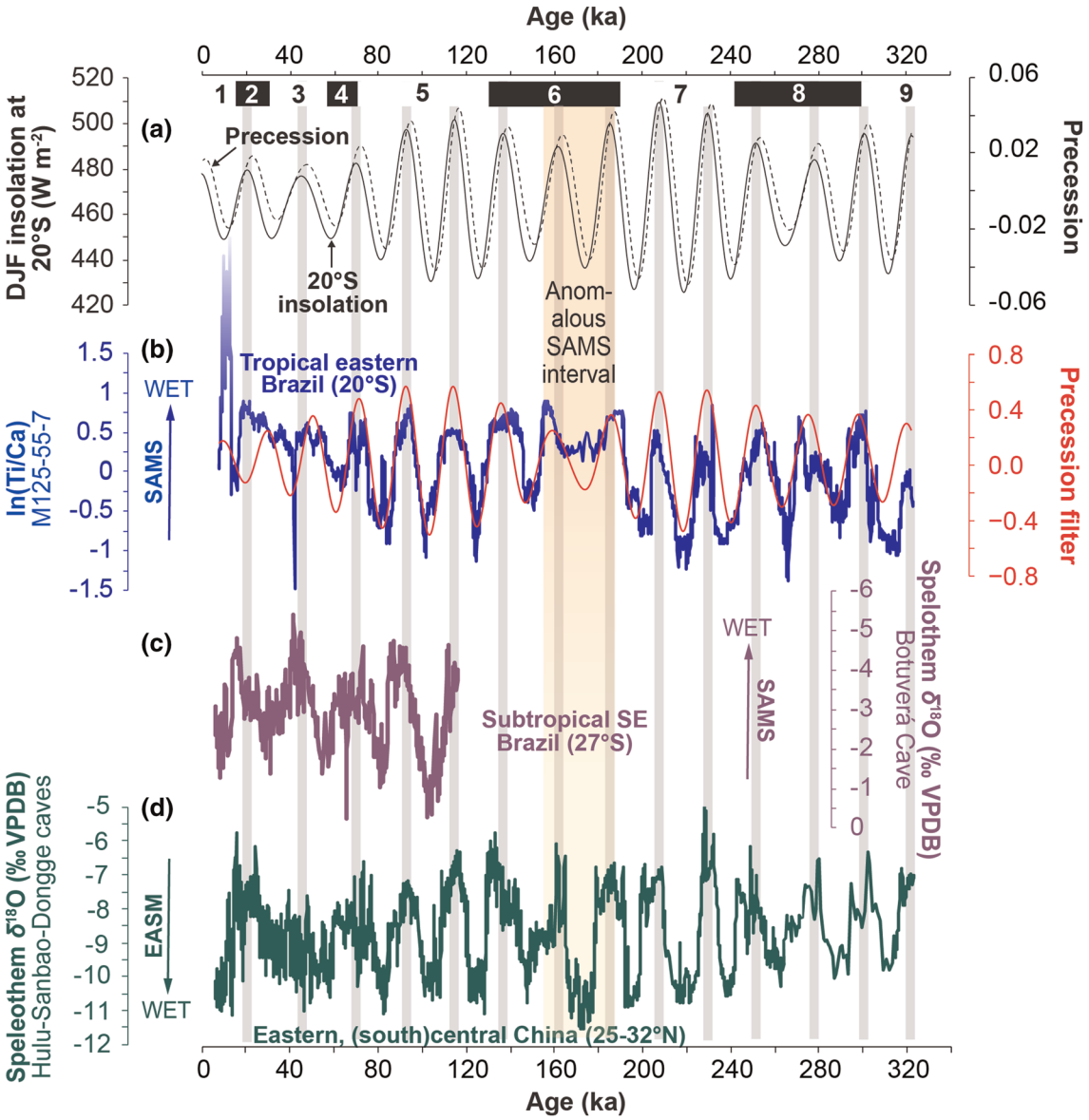

Figure 3. (a) Changes in austral summer (December-January-February [DJF]) insolation at 20°S (solid line) and orbital precession (dashed line) (Laskar et al., 2004). (b) ln (Ti/Ca) ratios based on X-ray fluorescence scanning of Core M125-55-7 (blue line) and the filtered ~23 Kyr signal from the Ti/Ca record (red line). (c) South American Monsoon System (SAMS) precipitation based on speleothem stable oxygen isotopes ($\delta^{18}O$) from Botuverá Cave (subtropical southeastern Brazil; Cruz et al., 2005) (purple line). (d) East Asian Summer Monsoon (EASM) precipitation based on stacked speleothem $\delta^{18}O$ records from Hulu, Dongge, and Sanbao caves in eastern, southcentral, and central China, respectively (green line) (Cheng et al., 2009; Dykoski et al., 2005; Kelly et al., 2006; Wang et al., 2001, 2008; Yuan et al., 2004). Gray bars denote peaks in austral summer insolation. The orange bar denotes an interval of Marine Isotope Stage 6 during which variability in M125-55-7 ln (Ti/Ca) ratios deviate from insolation changes. Numbers at the top indicate Marine Isotope Stages 1–9.

55-7 (western tropical South Atlantic) *G. ruber* (pink) Mg/Ca-based SST record (Hou et al., 2020) (Figures S8a and S8b). For computing the intrahemispheric temperature gradient, we utilized Site M125-55-7 SSTs and Site PS2489 (subantarctic zone) faunal SSTs (Becquey & Gersonde, 2003) (Figures S8b and S8c).

In line with modeling results (Rind, 1998, 2000), we find that the interhemispheric and intrahemispheric SST gradients increase (decrease) when atmospheric pCO_2 is lower (higher) (Figures S5c and S5d). Moreover, the increase in these latitudinal temperature gradients is associated with enhanced precipitation over the Doce Basin (Figures S5e and S5f). This agrees with model simulations which indicate that stronger

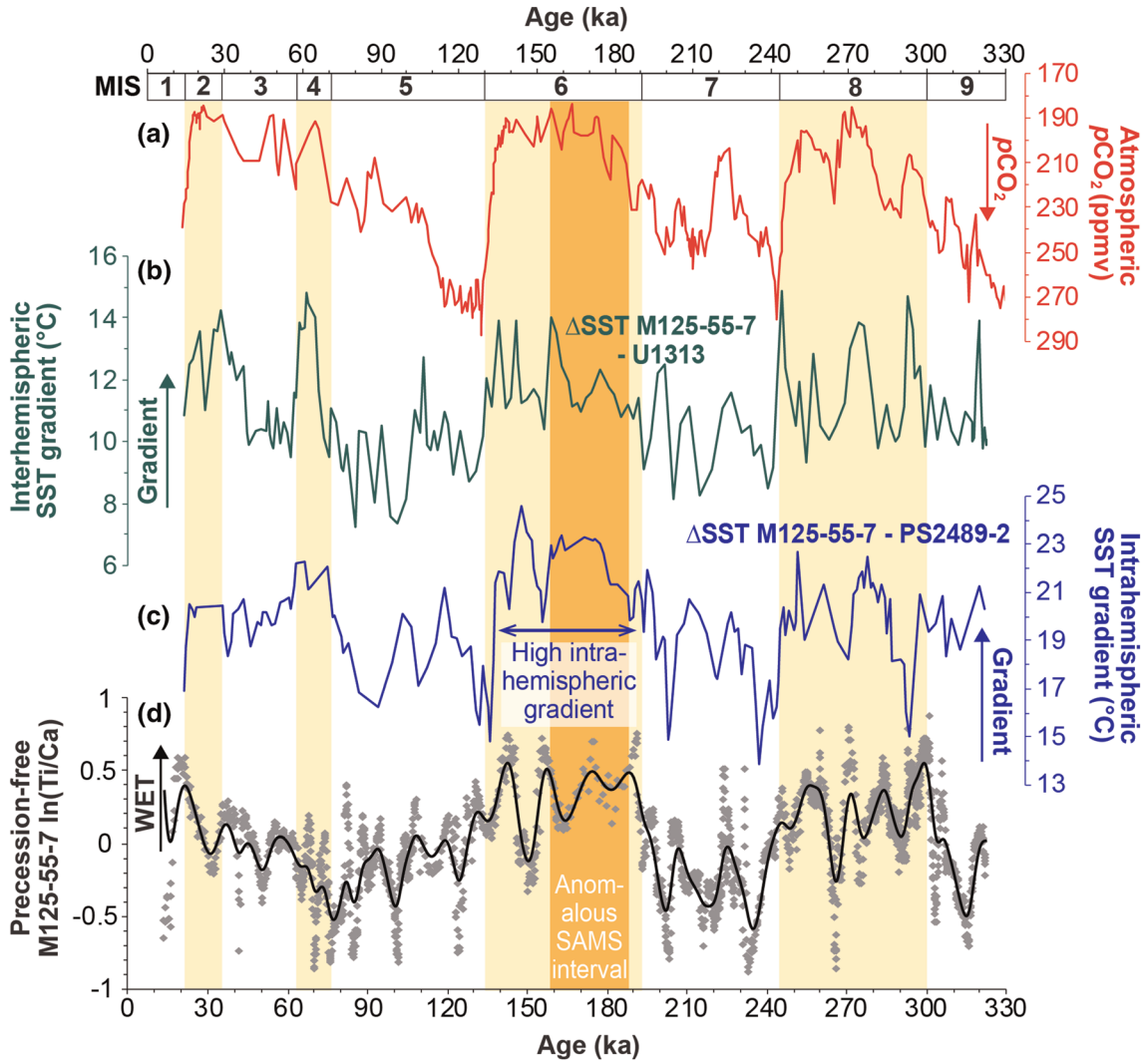

Figure 4. (a) Atmospheric pCO_2 (red line) (EPICA Dome C, Monnin et al., 2001; Vostok, Petit et al., 1999) (note reversed scale). (b) Interhemispheric Atlantic sea surface temperature (SST) gradient between Sites M125-55-7 (western tropical South Atlantic; Hou et al., 2020) and U1313 (midlatitude North Atlantic; Naafs et al., 2012) (green line). (c) South Atlantic intrahemispheric SST gradient between Sites M125-55-7 and PS2489-2 (subantarctic zone; Becquey & Gersonde, 2003) (blue line). (d) Smoothing Spline smoothed (black line; smoothing = 5) and raw precession-free (gray markers) ln (Ti/Ca) record based on X-ray fluorescence scanning of Core M125-55-7 (black line). Yellow bars and numbers at the top denote Marine Isotope Stages (MIS). The orange bar shows the interval of anomalous SAMS response to insolation forcing (see section 4.2).

latitudinal temperature gradients intensify the Hadley circulation (Held & Hou, 1980; Seo et al., 2014) and increase moisture availability in the (sub)tropics (Rind, 1998). A steeper intrahemispheric temperature gradient leads to intensified wintertime SE trade winds (Liu & Yang, 2003), thereby enhancing landward moisture advection and resulting in an increase in austral winter precipitation along of the coast of eastern Brazil (e.g., during the interval of weak SAMS response to insolation forcing; Figure 4c). The interhemispheric SST gradient has been shown to modulate the latitudinal position of the SACZ (Stríkis et al., 2015), which affects austral summer precipitation in the Doce Basin, since it is located at the NE extent of the SACZ and therefore sensitive to displacements in its location. This may explain the periodic differences in SAMS rainfall between the Doce Basin and the subtropical Botuverá Cave (e.g., over the last ~50 Kyr), where a northward displacement of the SACZ promotes enhanced rainfall at the NE SACZ boundary and subtropical drying (and vice versa for a southward shift of the SACZ) (Cruz et al., 2005, 2006) (Figures 3b and 3c). Thus, we propose that GHG may indirectly modulate SAMS precipitation through initial modifications to both the interhemispheric and intrahemispheric temperature gradients. Our findings

therefore suggest that monsoonal precipitation in tropical eastern Brazil is likely to decrease in the future, owing largely to the indirect effects of rising GHG concentrations.

4.4. MIS 6

As previously discussed, during MIS 6, the long-term anticorrelation between M125-55-7 ln (Ti/Ca) ratios and $\delta^{18}O_{ivf\text{-}sw}$ values reverses, and the tight coupling between the ln (Ti/Ca) record and austral summer insolation weakens (Figures 2 and 3a). We propose that exceptionally high Southern Hemisphere intrahemispheric SST gradients during this period led to anomalously strong wintertime SE trade winds, which caused prolonged SST warming in the western tropical South Atlantic due to the accumulation of wind-advected warm-water masses (Hou et al., 2020). The intensified SE trades also increased both wintertime moisture advection from the western South Atlantic to the eastern Brazilian coast and wind-driven evaporation in the western tropical South Atlantic. This led to more positive $\delta^{18}O_{IVF\text{-}SW}$ values and higher ln (Ti/Ca) ratios due to enhanced wintertime coastal rainfall (Figure 4c). Thus, austral winter precipitation may have had a stronger influence on ln (Ti/Ca) ratios than SAMS precipitation during this period, explaining the anomalous ln (Ti/Ca) ratio response to austral summer insolation forcing during MIS 6.

5. Conclusions

Our 322 Kyr ln (Ti/Ca) record traces continuous changes in rainfall intensity across tropical eastern Brazil and finds insolation forcing to be the dominant pacemaker of long-term SAMS variability, despite its high spatial complexity. Additionally, we find that the intensity of SAMS rainfall responds negatively to GHG forcing, through indirect mechanisms. We propose that GHG forcing directly influences the interhemispheric and intrahemispheric latitudinal temperature gradients, which in turn modify the strength of tropical atmospheric circulation and precipitation. During MIS 6, we discern an anomalous muted SAMS response to insolation forcing and a shift from the typical out-of-phase relationship between ln (Ti/Ca) and $\delta^{18}O_{IVF\text{-}SW}$ values. We attribute this to exceptionally strong wintertime SE trade winds which caused austral winter precipitation to dominate the ln (Ti/Ca) record. Our findings suggest that SAMS rainfall intensity over tropical eastern Brazil will likely decrease due to the anthropogenic-related rise in GHG concentrations. This will likely have important implications for government decisions regarding the timely adoption of mitigation strategies in the near future.

Data Availability Statement

The original data reported here are available online (https://doi.pangaea.de/10.1594/PANGAEA.914302).

Acknowledgments

We kindly acknowledge the captain and crew of the R/V METEOR during Expedition M125. We thank Stefanie Kaboth-Bahr for assistance with XRF scanning, Robert van Geldern for help with water isotope analysis, and Bernd Knape and Frank Keppler for support during foraminiferal stable isotope measurements. A. B. was funded by the Deutsche Forschungsgemeinschaft (DFG) (Grant BA 3809/9-1). C. M. C. was funded by FAPESP (Grant 2018/15123-4), CAPES (Grants 564/2015 and 88881.313535/2019-01), CNPq (Grants 302607/2016-1 and 422255/2016-5), and the Alexander von Humboldt Foundation.

References

Aguiar, A. L., Cirano, M., Pereira, J., & Marta-Almeida, M. (2014). Upwelling processes along a western boundary current in the Abrolhos-Campos region of Brazil. *Continental Shelf Research*, *85*, 42–59. https://doi.org/10.1016/j.csr.2014.04.013

Alvares, C. A., Stape, J. L., Sentelhas, P. C., De Moraes Gonçalves, J. L., & Sparovek, G. (2013). Köppen's climate classification map for Brazil. *Meteorologische Zeitschrift*, *22*(6), 711–728. https://doi.org/10.1127/0941-2948/2013/0507

Arz, H. W., Pätzold, J., & Wefer, G. (1998). Correlated millennial-scale changes in surface hydrography and terrigenous sediment yield inferred from Last-Glacial marine deposits off northeastern Brazil. *Quaternary Research*, *50*(2), 157–166. https://doi.org/10.1006/qres.1998.1992

Bahr, A., Albuquerque, A.L., Ardenghi, N., Batenburg, S.J., Bayer, M., Catunda, M.C., et al. (2016). South American hydrological balance and paleoceanography during the Late Pleistocene and Holocene (SAMBA) – Cruise No. M125 – March 21 – April 15, 2016 - Rio de Janeiro (Brazil) – Fortaleza (Brazil). METEOR-Berichte, M125, 47 pp., DFG-Senatskommission für Ozeanographie. https://doi.org/10.2312/cr_m125

Bahr, A., Schönfeld, J., Hoffmann, J., Voigt, S., Aurahs, R., Kucera, M., et al. (2013). Comparison of Ba/Ca and $\delta^{18}O_{WATER}$ as freshwater proxies: A multi-species core-top study on planktonic foraminifera from the vicinity of the Orinoco River mouth. *Earth and Planetary Science Letters*, *383*, 45–57. https://doi.org/10.1016/j.epsl.2013.09.036

Becquey, S., & Gersonde, R. (2003). A 0.55-Ma paleotemperature record from the subantarctic zone: Implications for Antarctic circumpolar current development. *Paleoceanography*, *18*(1), 1014. https://doi.org/10.1029/2000PA000576

Brand, W. A., Coplen, T. B., Vogl, J., Rosner, M., & Prohaska, T. (2014). Assessment of international reference materials for isotope-ratio analysis (IUPAC Technical Report). *Pure and Applied Chemistry*, *86*(3), 425–467. https://doi.org/10.1515/pac-2013-1023

Carvalho, L. M. V., Jones, C., & Liebmann, B. (2002). Extreme precipitation events in southeastern South America and large-scale convective patterns in the South Atlantic covergence zone. *Journal of Climate*, *15*(17), 2377–2394. https://doi.org/10.1175/1520-0442(2002)015<2377:EPEISS>2.0.CO;2

Carvalho, L. M. V., Jones, C., & Liebmann, B. (2004). The South Atlantic convergence zone: Intensity, form, persistence, and relationships with intraseasonal to interannual activity and extreme rainfall. *Journal of Climate*, *17*(1), 88–108. https://doi.org/10.1175/1520-0442(2004)017<0088:TSACZI>2.0.CO;2

Cheng, H., Edwards, R. L., Broecker, W. S., Denton, G. H., Kong, X., Wang, Y., et al. (2009). Ice age terminations. *Science*, *326*(5950), 248–252. https://doi.org/10.1126/science.1177840

Cheng, H., Sinha, A., Cruz, F. W., Wang, X., Edwards, R. L., d'Horta, F. M., et al. (2013). Climate change patterns in Amazonia and biodiversity. *Nature Communications*, *4*(1), 1411. https://doi.org/10.1038/ncomms2415

Cheng, H., Sinha, A., Wang, X., Cruz, F. W., & Edwards, R. L. (2012). The global paleomonsoon as seen through speleothem records from Asia and the Americas. *Climate Dynamics*, *39*(5), 1045–1062. https://doi.org/10.1007/s00382-012-1363-7

Coplen, T. B. (2011). Guidelines and recommended terms for expression of stable-isotope-ratio and gas ratio measurement results. *Rapid Communications in Mass Spectrometry*, *25*(17), 2538–2560. https://doi.org/10.1002/rcm.5129

Cruz, F. W., Burns, S. J., Karmann, I., Sharp, W. D., & Vuille, M. (2006). Reconstruction of regional atmospheric circulation features during the late Pleistocene in subtropical Brazil from oxygen isotope composition of speleothems. *Earth and Planetary Science Letters*, *248*(1–2), 495–507. https://doi.org/10.1016/j.epsl.2006.06.019

Cruz, F. W., Burns, S. J., Karmann, I., Sharp, W. D., Vuille, M., Cardoso, A. O., et al. (2005). Insolation-driven changes in atmospheric circulation over the past 116,000 years in subtropical Brazil. *Nature*, *434*(7029), 63–66. https://doi.org/10.1038/nature03365

Dekens, P. S., Lea, D. W., Pak, D. K., & Spero, H. J. (2002). Core top calibration of Mg/Ca in tropical foraminifera: Refining paleotemperature estimation. *Geochemistry, Geophysics, Geosystems*, *3*(4), 1–29. https://doi.org/10.1029/2001gc000200

de Boer, B., Lourens, L. J., & de Wal, R. S. W. (2014). Persistent 400,000-year variability of Antarctic ice volume and the carbon-cycle is revealed throughout the Plio-Pleistocene. *Nature Communications*, *5*(1), 2999. https://doi.org/10.1038/ncomms3999

de Castro, B. M., Brandini, F. P., Pires-Vanin, A. M. S., & Miranda, L. B. (2006). Multidisciplinary oceanographic processes on the Western Atlantic continental shelf between 4°N and 34°S. *The Sea, Volume 14A: The Global Coastal Ocean*, *14A*(2016), 259–294.

Dykoski, C. A., Edwards, R. L., Cheng, H., Yuan, D., Cai, Y., Zhang, M., et al. (2005). A high-resolution, absolute-dated Holocene and deglacial Asian monsoon record from Dongge Cave, China. *Earth and Planetary Science Letters*, *233*(1–2), 71–86. https://doi.org/10.1016/j.epsl.2005.01.036

Gan, M. A., Kousky, V. E., & Ropelewski, C. F. (2004). The South America monsoon circulation and its relationship to rainfall over west-central Brazil. *Journal of Climate*, *17*(1), 47–66. https://doi.org/10.1175/1520-0442(2004)017<0047:TSAMCA>2.0.CO;2

Gouhier, T.C., Grinsted, A., Simko, V. (2019). R package biwavelet: Conduct univariate and bivariate wavelet analyses (Version 0.20.19). Available from https://github.com/tgouhier/biwavelet

Govin, A., Chiessi, C. M., Zabel, M., Sawakuchi, A. O., Heslop, D., Hörner, T., et al. (2014). Terrigenous input off northern South America driven by changes in Amazonian climate and the North Brazil current retroflection during the last 250 ka. *Climate of the Past*, *10*(2), 843–862. https://doi.org/10.5194/cp-10-843-2014

Govin, A., Holzwarth, U., Heslop, D., Ford Keeling, L., Zabel, M., Mulitza, S., et al. (2012). Distribution of major elements in Atlantic surface sediments (36°N-49°S): Imprint of terrigenous input and continental weathering. *Geochemistry, Geophysics, Geosystems*, *13*, Q01013. https://doi.org/10.1029/2011GC003785

Hammer, Ø., Harper, D. A. T., & Ryan, P. D. (2001). Past: Paleontological statistics software package for education and data analysis. *Palaeontologia Electronica*, *4*(1), 178. Retrieved from. http://palaeo-electronica.orghttp//palaeo-electronica.org/2001_1/past/issue1_01.htm

Held, I. M., & Hou, A. Y. (1980). Nonlinear axially symmetric circulations in a nearly inviscid atmosphere. *Journal of the Atmospheric Sciences*, *37*(3), 515–533. https://doi.org/10.1175/1520-0469(1980)037<0515:NASCIA>2.0.CO;2

Hou, A., Bahr, A., Schmidt, S., Strebl, C., Albuquerque, A. L., Chiessi, C. M., & Friedrich, O. (2020). Forcing of western tropical South Atlantic sea surface temperature across three glacial-interglacial cycles. *Global and Planetary Change*, *188*, 103150. https://doi.org/10.1016/j.gloplacha.2020.103150

Jaeschke, A., Rühlemann, C., Arz, H. W., Heil, G., & Lohmann, G. (2007). Coupling of millennial-scale changes in sea surface temperature and precipitation off northeastern Brazil with high-latitude climate shifts during the last glacial period. *Paleoceanography*, *22*, PA4206. https://doi.org/10.1029/2006PA001391

Kelly, M. J., Edwards, R. L., Cheng, H., Yuan, D., Cai, Y., Zhang, M., et al. (2006). High resolution characterization of the Asian monsoon between 146,000 and 99,000 years B.P. from Dongge Cave, China and global correlation of events surrounding Termination II. *Palaeogeography, Palaeoclimatology, Palaeoecology*, *236*(1–2), 20–38. https://doi.org/10.1016/j.palaeo.2005.11.042

Kutzbach, J. E. (1981). Monsoon climate of the Early Holocene: Climate experiment with the Earth's orbital parameters for 9000 years ago. *Science*, *214*(4516), 59–61. https://doi.org/10.1126/science.214.4516.59

Kutzbach, J. E., Liu, X., Liu, Z., & Chen, G. (2008). Simulation of the evolutionary response of global summer monsoons to orbital forcing over the past 280,000 years. *Climate Dynamics*, *30*(6), 567–579. https://doi.org/10.1007/s00382-007-0308-z

Laskar, J., Robutel, P., Joutel, F., Gastineau, M., Correia, A. C. M., & Levrard, B. (2004). A long-term numerical solution for the insolation quantities of the Earth. *Astronomy and Astrophysics*, *428*(1), 261–285. https://doi.org/10.1051/0004-6361:20041335

Liebmann, B., & Mechoso, C. R. (2011). The South American Monsoon System. In C. P. Chang, et al. (Eds.), *The Global Monsoon System: Research and forecast* (2nd ed., pp. 137–157). Singapore: World scientific publishing.

Lisiecki, L. E., & Raymo, M. E. (2005). A Pliocene-Pleistocene stack of 57 globally distributed benthic $\delta^{18}O$ records. *Paleoceanography*, *20*, PA1003. https://doi.org/10.1029/2004PA001071

Liu, Z., & Yang, H. (2003). Extratropical control of tropical climate, the atmospheric bridge and oceanic tunnel. *Geophysical Research Letters*, *30*(5), 1230. https://doi.org/10.1029/2002gl016492

Marengo, J. A., Liebmann, B., Grimm, A. M., Misra, V., Silva Dias, P. L., Cavalcanti, I. F. A., et al. (2012). Recent developments on the South American monsoon system. *International Journal of Climatology*, *32*(1), 1–21. https://doi.org/10.1002/joc.2254

Marengo, J. A., Liebmann, B., Kousky, V. E., Filizola, N. P., & Wainer, I. C. (2001). Onset and end of the rainy season in the Brazilian Amazon Basin. *Journal of Climate*, *14*(5), 833–852. https://doi.org/10.1175/1520-0442(2001)014<0833:OAEOTR>2.0.CO;2

Meyers, S. R. (2014). Astrochron: An R package for astrochronology. https://cran.r-project.org/package=astrochron

Monnin, E., Indermühle, A., Dällenbach, A., Flückiger, J., Stauffer, B., Stocker, T. F., et al. (2001). Atmospheric CO_2 concentrations over the last glacial termination. *Science*, *291*(5501), 112–114. https://doi.org/10.1126/science.291.5501.112

Mulitza, S., Boltovskoy, D., Donner, B., Meggers, H., Paul, A., & Wefer, G. (2003). Temperature: $\delta^{18}O$ relationships of planktonic foraminifera collected from surface waters. *Palaeogeography, Palaeoclimatology, Palaeoecology*, *202*(1-2), 143–152. https://doi.org/10.1016/S0031-0182(03)00633-3

Mulitza, S., Chiessi, C. M., Schefuß, E., Lippold, J., Wichmann, D., Antz, B., et al. (2017). Synchronous and proportional deglacial changes in Atlantic meridional overturning and northeast Brazilian precipitation. *Paleoceanography*, *32*, 622–633. https://doi.org/10.1002/2017PA003084

Naafs, B. D. A., Hefter, J., Acton, G., Haug, G. H., Martínez-Garcia, A., Pancost, R., & Stein, R. (2012). Strengthening of North American dust sources during the late Pliocene (2.7Ma). *Earth and Planetary Science Letters*, *317-318*, 8–19. https://doi.org/10.1016/j.epsl.2011.11.026

Oliveira, K. S. S., & da Silva Quaresma, V. (2017). Temporal variability in the suspended sediment load and streamflow of the Doce River. *Journal of South American Earth Sciences*, *78*, 101–115. https://doi.org/10.1016/j.jsames.2017.06.009

Pascale, S., Carvalho, L. M. V., Adams, D. K., Castro, C. L., & Cavalcanti, I. F. A. (2019). Current and future variations of the monsoons of the Americas in a warming climate. *Current Climate Change Reports*, *5*(3), 125–144. https://doi.org/10.1007/s40641-019-00135-w

Peterson, L. C., Haug, G. H., Hughen, K. A., & Rohl, U. (2000). Rapid changes in the hydrologic cycle of the tropical Atlantic during the last glacial. *Science*, *290*(5498), 1947–1951. https://doi.org/10.1126/science.290.5498.1947

Petit, J. R., Jouzel, J., Raynaud, D., Barkov, N. I., Barnola, J. M., Basile, I., et al. (1999, June). Climate and atmospheric history of the past 420,000 years from the Vostok ice core, Antarctica. *Nature*, *399*(6735), 429–436. https://doi.org/10.1038/20859

Rind, D. H. (1998). Latitudinal temperature gradients and climate change. *Journal of Geophysical Research*, *103*(D6), 5943–5971. https://doi.org/10.1029/97JD03649

Rind, D. H. (2000). Relating paleoclimate data and past temperature gradients: Some suggestive rules. *Quaternary Science Reviews*, *19*(1–5), 381–390. https://doi.org/10.1016/S0277-3791(99)00070-0

Rothwell, R., & Croudace, I. (2015). Twenty years of XRF core scanning marine sediments: What do geochemical proxies tell us? In I. Croudace & R. Rothwell (Eds.), *Micro-XRF studies of sediment cores. Developments in paleoenvironmental research* (Vol. 17, pp. 25–102). Dordrecht: Springer.

Rühlemann, C., Frank, M., Hale, W., Mangini, A., Mulitza, S., Müller, P. J., & Wefer, G. (1996). Late quaternary productivity changes in the western equatorial Atlantic: Evidence from ^{230}Th-normalized carbonate and organic carbon accumulation rates. *Marine Geology*, *135*(1–4), 127–152. https://doi.org/10.1016/S0025-3227(96)00048-5

Schlitzer, R. (2018). Ocean data view, http://odv.awi.de

Seo, K. H., Frierson, D. M. W., & Son, J. H. (2014). A mechanism for future changes in Hadley circulation strength in CMIP5 climate change simulations. *Geophysical Research Letters*, *41*, 5251–5258. https://doi.org/10.1002/2014GL060868

Silva, V.B.S., & Kousky, V.E. (2012). The South American Monsoon System: Climatology and variability. In S.-Y. Wang (Ed.), Modern Climatology. Retrieved from http://www.intechopen.com/books/modern-climatology/the-south-american-monsoon-system-climatology-and-variability

Stríkis, N. M., Chiessi, C. M., Cruz, F. W., Vuille, M., Cheng, H., de Souza Barreto, E. A., et al. (2015). Timing and structure of mega-SACZ events during Heinrich Stadial 1. *Geophysical Research Letters*, *42*, 5477–5484. https://doi.org/10.1002/2015GL064048

Thomson, D. J. (1982). Spectrum estimation and harmonic analysis. *Proceedings of the IEEE*, *70*(9), 1055–1096. https://doi.org/10.1109/proc.1982.12433

Vera, C. S., Higgins, W., Amador, J., Ambrizzi, T., Garreaud, R., Gochis, D., et al. (2006). Toward a unified view of the American monsoon systems. *Journal of Climate*, *19*(20), 4977–5000. https://doi.org/10.1175/JCLI3896.1

Vera, C. S., Vigliarolo, P. K., & Berbery, E. H. (2002). Cold season synoptic-scale waves over subtropical South America. *Monthly Weather Review*, *130*(3), 684–699. https://doi.org/10.1175/1520-0493(2002)130<0684:CSSSWO>2.0.CO;2

Volbers, A. N. A., & Henrich, R. (2004). Calcium carbonate corrosiveness in the South Atlantic during the Last Glacial Maximum as inferred from changes in the preservation of Globigerina bulloides: A proxy to determine deep-water circulation patterns? *Marine Geology*, *204*(1–2), 43–57. https://doi.org/10.1016/S0025-3227(03)00372-4

Vuille, M., Burns, S. J., Taylor, B. L., Cruz, F. W., Bird, B. W., Abbott, M. B., et al. (2012). A review of the South American monsoon history as recorded in stable isotopic proxies over the past two millennia. *Climate of the Past*, *8*(4), 1309–1321. https://doi.org/10.5194/cp-8-1309-2012

Wang, Y. J., Cheng, H., Edwards, R. L., An, Z. S., Wu, J. Y., Shen, C. C., & Dorale, J. A. (2001). A high-resolution absolute-dated Late Pleistocene monsoon record from Hulu Cave, China. *Science*, *294*(5550), 2345–2348. https://doi.org/10.1126/science.1064618

Wang, Y. J., Cheng, H., Edwards, R. L., Kong, X., Shao, X., Chen, S., et al. (2008). Millennial- and orbital-scale changes in the East Asian monsoon over the past 224,000 years. *Nature*, *451*(7182), 1090–1093. https://doi.org/10.1038/nature06692

Xie, P., & Arkin, P. A. (1997). A 17-year monthly analysis based on gauge observations, satellite estimates, and numerical model outputs. *Bulletin of the American Meteorological Society*, *78*(11), 2539–2558. Retrieved from. https://doi.org/10.1175/1520-0477%281997%29078%3C2539%3AGPAYMA%3E2.0.CO%3B2

Yu, L. (2007). Global variations in oceanic evaporation (1958-2005): The role of the changing wind speed. *Journal of Climate*, *20*(21), 5376–5390. https://doi.org/10.1175/2007JCLI1714.1

Yuan, D., Cheng, H., Edwards, R. L., Dykoski, C. A., Kelly, M. J., Zhang, M., et al. (2004). Timing, duration, and transitions of the last interglacial Asian monsoon. *Science*, *304*(5670), 575–578. https://doi.org/10.1126/science.1091220

Zhou, J., & Lau, K. M. (1998). Does a monsoon climate exist over South America? *Journal of Climate*, *11*(5), 1020–1040. https://doi.org/10.1175/1520-0442(1998)011<1020:DAMCEO>2.0.CO;2